Advances in Aircraft and Spacecraft Science, *Vol. 9, No. 3 (2022) 243-261*
https://doi.org/10.12989/aas.2022.9.3.243

Bending analysis of power-law sandwich FGM beams under thermal conditions

Aman Garg*[1], Mohamed-Ouejdi Belarbi[2], Li Li[3] and Abdelouahed Tounsi[4,5,6]

[1]Department of Civil and Environmental Engineering, The NorthCap University, Gurugram, Haryana, 122017, India
[2]Laboratoire de Génie Energétique et Matériaux, LGEM, Faculté de la Science et de lo Technologie, Université de Biskra, B.P. 145, R.P. 07000, Biskra, Algeria
[3]State Key Laboratory of Digital Manufacturing Equipment and Technology, School of Mechanical Science and Engineering, Huazhong University of Science and Technology, Wuhan 430074, China
[4]YFL (Yonsei Frontier Lab), Yonsei University, Seoul, Korea
[5]Department of Civil and Environmental Engineering, King Fahd University of Petroleum &Minerals, 31261 Dhahran, Eastern Province, Saudi Arabia
[6]Material and Hydrology Laboratory, Faculty of Technology, Civil Engineering Department, University of Sidi Bel Abbes, 22000 Sidi Bel Abbes, Algeria

(Received April 6, 2022, Revised April 21, 2022, Accepted May 18, 2022)

Abstract. Broad writing on the examination of sandwich structures mirrors the significance of incorporating thermal loadings during their investigation stage. In the current work, an endeavor has been made to concentrate on sandwich FGM beams' bending behaving under thermal loadings utilizing shear deformation theory. Temperature-dependent material properties are used during the analysis. The formulation includes the transverse displacement field, which helps better predict the behavior of thick FGM beams. Three-different thermal profiles across the thickness of the beam are assumed during the analysis. The study has been carried out on both symmetric and unsymmetric sandwich FGM beams. It has been observed that the bending behavior of sandwich FGM beams is impacted by the temperature profile to which it is subjected. Power-law exponent and thickness of core also affect the behavior of the beam.

Keywords: exponential; finite element; sandwich FGM beam; sigmoidal; thermal bending

1. Introduction

These days, sandwich structures are perhaps the most suitable types of cutting-edge composite design created by engineers. They comprise two thin face layers (or skins) of higher rigidity and a low-weight thick center layer of adequate transverse shear rigidity (Polat 2021). Sandwich structures have been pervasively applied in the current design, particularly in the civil, marine industry, aviation applications, and other modern applications, because of their great mechanical performances (i.e., high bending rigidity and vibration characteristics, high ratio of stiffness to weight, excellent durability). However, the sudden transition in mechanical and thermal properties at interfaces may prompt failure by delamination, plastic deformation, or cracking (Chareonsuk and

*Corresponding author, Assistant Professor, E-mail: amang321@gmail.com, amangarg@ncuindia.edu

Copyright © 2022 Techno-Press, Ltd.
http://www.techno-press.org/?journal=aas&subpage=7 ISSN: 2287-528X (Print), 2287-5271 (Online)

Vessakosol 2011, Thai *et al.* 2014, Yaylaci *et al.* 2021). Moreover, these classical sandwiches are incapable of employing in high-temperature environments (Ghatage *et al.* 2020). To beat these unfavorable impacts, another high-level class of materials, called Functionally Graded Materials (FGM), was proposed in 1984s by a gathering of Japanese researchers (Koizumi and Niino 1995). These materials are infinitesimally inhomogeneous in which the mechanical properties fluctuate without a hitch and persistently from one surface to the next (Natarajan and Manickam 2012, Reddy 2000). Generally, the FGM is made from a mixture of ceramic and metal (Singh and Azam 2021). The metal constituent gives durability and mechanical strength, and the ceramic constituent of the material gives high-temperature obstruction because of its low thermal conductivity (Ma *et al.* 2021). Hosseini (2020) presented exact solutions for the analysis of nano FG beams.

Equivalent single-layer theories (ESL), layerwise (LW) theories, zigzag theories (ZZ), continuity-based 3D elasticity theories, and unified formulations are the major categories under which the available theories for the analysis of FGM beams can be classified. The simplest ESL is called as classical Euler-Bernoulli beam theory (CBT). With the help of CBT, Zhao and Yu (2021) carried out the analysis of axially FG beams. The CBT ignores the transverse shear strain and is suitable only to study slender beams (Civalek and Demir 2011, Ghannadpour *et al.* 2013, Nejad *et al.* 2018). However, it is not appropriate for the moderately thick and thick beams, requiring that the transverse and normal strain be considered. First-order shear deformation beam theory (FSDT), also called the Timoshenko beam theory (TBT), is an improvement over CBT. Bekhadda *et al*. (2019) employed FSDT to analyze FGM beams. The TBT considers the transverse shear deformation impacts and gives satisfactory outcomes for short and thin bars. Free vibration behavior of FG piezoelectric nanobeams was carried out by Huang and Tahouneh (2021) in the framework of TBT. Akbaş (2021) carried out the dynamic analysis of FG beams subjected to moving load. Wang *et al.* (2021) employed the principles of FSDT for buckling analysis of FG nanobeams. Transient analysis of porous sandwich FG plates was carried out by Esmaeilzadeh *et al.* 2021 using FSDT under the effects of moving loads. With the help of finite element-based TBT, Almitani *et al.* 2021 carried out stress and vibration analysis of axially graded FG beams. Notwithstanding, it needs a shear correction factor, which is difficult to come by as it relies upon the calculations, material properties, and end conditions (Abualnour *et al.* 2018, Wu and Li 2021).

To conquer the restriction of CBT and TBT, different higher-order shear deformation theories (HSDTs) (sinusoidal, exponential, hyperbolic, inverse-hyperbolic, and third-order shear deformation theory) are available (Thai and Vo 2012, Filippi *et al.* 2015, Bennai *et al.* 2015). They do now not require any shear correction factor. These theories include higher-order phrases in approximating the in-plane displacement fields and fulfilling zero transverse shear stress conditions at the top and base surfaces of the beam. Many computational models, each analytically and numerically, have been proposed to expect the mechanical/thermal conduct of FGM sandwich beams as it should be. Bouafia *et al.* (2021) proposed quasi 3D HSDT to analyze FG plates resting on an elastic foundation. Kouider *et al.* (2021) proposed HSDT for bending and vibration analysis of FG plates. Tahir (2022) analyzed FGM plates using quasi 3D HSDT.

Several articles are available in the literature regarding the analysis of FGM beams using HSDT. Plenty of them is on the mechanical loading-based analysis of FGM and sandwich FGM beams. A detailed review of sandwich FGM beams analysis is available in the review work published by Sayyad and Ghugal (2019) and Garg *et al.* (2021a, b). Based on the review mentioned review works, it is easy to see that the literature on the analysis of the static response of FGM sandwich beams under mechanical loading is plenty. However, the research on static bending of FGM beams under thermal loadings is quite limited. Kadoli *et al.* (2008) presented a new finite element beam

formulation based on TSDT to analyze the static behavior of FGM beams under ambient temperature. Natarajan and Manickam (2012) investigated the bending and free vibration responses of FGM sandwich plates under mechanical/thermal loadings using a new Co eight noded quadrilateral element based on HSDT. Later, Wattanasakulpong *et al.* (2011) used Shi's TSDT (Shi 2007) to investigate the functionally graded beams' thermal buckling and free vibration analysis. The same authors used the same solution methodology for functionally graded plates' free and forced vibration responses under high-temperature loading (Wattanasakulpong *et al.* 2013). Majumdar and Das (2018) used CBT to study the thermal buckling response of clamped FGM beams under linear and nonlinear thermal gradient across the thickness. Based on HSDT, Babaei *et al.* (2018) carried out a nonlinear bending analysis of the FGM curved tube under a thermal environment. Rezaiee-Pajand *et al.* (2020) proposed an efficient four-nodes isoparametric beam element for thermo-mechanical nonlinear analysis of FGM porous beams. Tran *et al.* (2021) carried out static bending and buckling FGM sandwich beam responses under high temperature using a two-noded Hermite-Lagrangian finite element based on a new TSDT. Madenci and Ozkili (2021) presented the free vibration-based results of porous FG beams obtained using analytical, numerical, and artificial neural network techniques. Madenci (2021a, b) presented mixed finite element-based HSDT for analysis of FG beams. Ebrahimi *et al.* 2021 proposed four-variable-based HSDT to analyze FG carbon nanotubes reinforced composite plates. With the help of finite element-based HSDT, Sahoo *et al.* 2021 carried out a buckling analysis of FG shells under thermal conditions. Farrokh and Taheripur (2021) optimized the distribution of porosities across the thickness of the FG porous beams. Hadji *et al*. (2022) employed HSDT for thermal buckling analysis of porous FG plates.

From the previous literature survey, many ESL theories were used in the analysis of the FGM sandwich structures under mechanical/thermal conditions. The main advantages of ESL theories are their inherent simplicity and low computational cost because the number of variables is independent of the number of layers. However, ESL theories fail to precisely capture the local behavior of FGM sandwich structures (Carrera 2003, Li 2020). To overcome the limitations of ESL theories, layerwise and zigzag theories have been used. Each layer is treated separately in these theories. The variables are linked to specific layers (Belarbi *et al.* 2017, Di Sciuva and Sorrenti 2021, Dorduncu 2020, Garg *et al.* 2020a, b, Garg and Chalak 2019, 2020, Pandey and Pradyumna 2018a, b). The zigzag function can accurately predict the global and local responses of composite laminated and FGM structures. However, these zigzag theories are computationally costlier as compared to the HSDTs.

The novelty of the present work: From the review available on the analysis of sandwich FGM beams, it has been observed that several articles are available on the thermal-based analysis of FGM beams, but very few are available on predicting the bending behavior of sandwich FGM beams. Even most works assumed a uniform distribution of temperature across the entire beam thickness. In the present work, analytical solutions-based parabolic shear deformation theory has been applied for the bending analysis of sandwich FGM beams under different thermal loadings. The proposed theory incorporates the transverse displacement field. Three different thermal conditions: equal rise and fall of temperature at the top and bottom surfaces of the beam, equal rise and fall of temperature, and unequal rise and fall of temperature at the top and bottom surfaces of the beam are considered. Temperature-dependent material properties are considered during the analysis. It has been observed that the assumed thermal condition widely affects the bending behavior of the beam.

2. Mathematical and material modeling

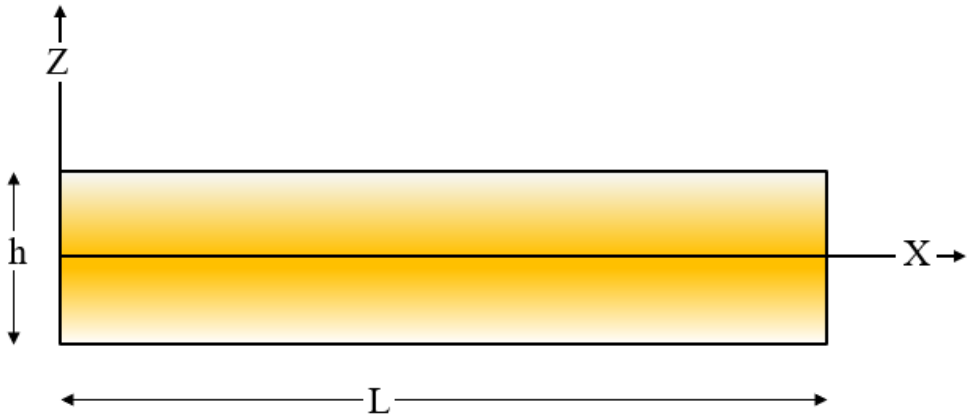

Fig. 1 Geometry of sandwich FGM beam

The in-plane and transverse displacement fields for a beam of length L units and height h units (Fig. 1) can be expressed as

$$\begin{gathered} u(x,z) = u_0(x) - z\frac{\partial w_b}{\partial x} - f(z)\frac{\partial w_s}{\partial x} \\ w(x,z) = w_b(x) + w_s(x) \end{gathered} \tag{1}$$

where u_0 is the mid-plane displacement, w_s and w_b are the bending and shear components of transverse displacement. $f(z)$ is a shape function affecting the distribution of transverse shear stresses across the thickness of the beam adopted as:

$$f(z) = z\left(1 - \frac{3}{2}\left(\frac{z}{h}\right)^2 + \frac{2}{5}\left(\frac{z}{h}\right)^4\right) \tag{2}$$

The strain-displacement relationships can be stated as

$$\begin{gathered} \varepsilon_x = \varepsilon_x^0 + zk_x^b + f(z)k_x^s \\ \gamma_{xz} = g(z)\gamma_{xz}^s \\ \varepsilon_z = 0 \end{gathered} \tag{3}$$

where

$$\varepsilon_x^0 = \frac{\partial u_0}{\partial x},\ k_x^b = -\frac{\partial^2 w_b}{\partial x^2},\ k_x^s = -\frac{\partial^2 w_s}{\partial x^2},\ \gamma_{xz}^s = \frac{\partial w_s}{\partial x},\ g(z) = 1 - f'(z).$$

The linear constitutive relationship considering thermal conditions can be expressed as

$$\{\sigma\} = [Q] - \{\varepsilon_s - \alpha\Delta T\} \tag{4}$$

Using the principle of virtual work, the equilibrium equation can be expressed as

$$\int_{-h/2}^{h/2}\int_{\psi}[\sigma_x\delta\varepsilon_x + \tau_{xz}\delta\gamma_{xz}]d\psi\, dz - \int_{\psi} q\delta w d\psi \tag{5}$$

where ψ is the top surface and q denotes the load applied.

Substituting Eqs. (3) and (4) in Eq. (5), we get

$$\int_{\psi}[N_x\delta\varepsilon_x^0 + M_x^b\delta k_x^b + M_x^s\delta k_x^s + +S_{xz}^s\delta\gamma_{xz}^s]d\psi - \int_{\psi} q\delta w d\psi \tag{6}$$

where

$$\begin{Bmatrix} N_x \\ M_x^b \\ M_x^s \end{Bmatrix} = \int_{-h/2}^{h/2} (\sigma_x) \begin{Bmatrix} 1 \\ z \\ f(z) \end{Bmatrix} dz,\ S_{xz}^s = \int_{-h/2}^{h/2} \tau_{xz} g(z) dz.$$

Performing integration by parts over Eq. (6) and equating the coefficients to zero, one can obtain

$$\begin{gathered} \delta u: \frac{\partial N_x}{\partial x} = 0 \\ \delta w_b: \frac{\partial^2 M_x^b}{\partial x^2} + q = 0 \\ \delta w_s: \frac{\partial^2 M_x^s}{\partial x^2} + \frac{\partial S_{xz}^s}{\partial x} + q = 0 \end{gathered} \tag{7}$$

Using Eq. (4) in Eq. (10), the stress resultants can be related to total strains as

$$\begin{Bmatrix} N_x \\ M_x^b \\ M_x^s \end{Bmatrix} = \begin{bmatrix} A & B & B^s \\ A & D & D^s \\ B^s & D^s & H^s \end{bmatrix} \begin{Bmatrix} \varepsilon_x^0 \\ k_x^b \\ k_x^s \end{Bmatrix},\ \{S_{xz}^s\} = [A^s]\{\gamma_{xz}\} \tag{8}$$

where

$$\{A \quad B \quad D \quad B^s \quad D^s \quad H^s\} = \int_{-h/2}^{h/2} Q_{11}\left(1, z, z^2, f(z), zf(z), f^2(z)\right) dz,$$

$$A^s = \int_{h_{n-1}}^{h_n} Q_{55}[g(z)]^2 dz.$$

Substituting Eq. (8) in Eq. (7), we get

$$\begin{gathered} Au_0 - Bd_{111}w_b - B^s d_{111}w_s = 0 \\ Bd_{111}u_0 - Dd_{1111}w_b - D^s d_{1111}w_s = q \\ B^s d_{111}u_0 - D^s d_{1111}w_b - H^s d_{1111}w_s + A^s d_{11}w_s = q \end{gathered} \tag{9}$$

For simply supported boundary conditions, $w_b = w_s = N_x = M_x^b = M_x^s = 0$. Navier solutions are assumed to satisfy the boundary conditions as

$$\begin{Bmatrix} u_0 \\ w_b \\ w_s \end{Bmatrix} = \begin{Bmatrix} U\cos(\lambda x) \\ W_b \sin(\lambda x) \\ W_s \sin(\lambda x) \end{Bmatrix} \tag{10}$$

where $\lambda = \pi/a$. One obtains the following operator equation

$$[C]\{\Delta\} = \{P\} \tag{11}$$

where $\{\Delta\} = \{u_0\ w_b\ w_s\}^T$ and $[C] = \begin{bmatrix} a_{11}a_{12}a_{13} \\ a_{12}a_{22}a_{23} \\ a_{13}a_{23}a_{33} \end{bmatrix}$, $a_{11} = A\lambda^2$, $a_{12} = -B\lambda^3$, $a_{13} = -B^s\lambda^3$, $a_{22} = D\lambda^4$, $a_{23} = D^s\lambda^4$, $a_{33} = H^s\lambda^2$.

For modeling sandwich FGM plates, power-law is used as

Type-A: Core made of ceramic and top and bottom faces of FGM: H-Type-A (Hardcore-Type-A); Core made of metal and top and bottom faces of FGM: S-Type-A (Softcore-Type-A).

Type-B: Core made of FGM, top and bottom faces of ceramic and metal, respectively called CT-Type-B. The top and bottom faces are made of metal and ceramic, respectively, called MT-Type-B plates.

$$P(z) = P_m + (P_c - P_m)V_c(z).$$

Type A: $V_c(z) = \left(\frac{z-h_0}{h_1-h_0}\right)^n$ for $z \in [h_0, h_1]$, $V_c(z) = 1$ for $z \in [h_1, h_2]$, $V_c(z) = \left(\frac{z-h_3}{h_2-h_3}\right)^n$ for $z \in [h_2, h_3]$

Type B: $V_c(z) = 0$ for $z \in [h_0, h_1]$, $V_c(z) = \left(\frac{z-h_1}{h_2-h_1}\right)^n$ for $z \in [h_1, h_2]$, $V_c(z) = 1$ for $z \in [h_2, h_3]$.

3. Results and discussion

Following temperature distributions are assumed at the top and bottom surfaces on the beam with linear variation across the thickness of the beam.

Case A: Equal rise and fall of temperature at the top and bottom surfaces of the beam $T_u = -T_l = T_0 \sin\frac{\pi x}{L}$.

Case B: Equal rise of temperature at the top and bottom surfaces of the beam $\left(T_u = T_l = T_0 \sin\frac{\pi x}{L}\right)$.

Case C: Unequal rise of temperature at the top and bottom surfaces of the beam $\left(T_u = T_0 \sin\frac{\pi x}{L};\ T_l = T_{01} \sin\frac{\pi x}{L}\right)$.

$T_0 = 100, T_{01} = 200$.

Non-dimensional deflection $\bar{w}\left(\frac{L}{2}, 0\right) = \frac{\mathrm{w}(L/2,0)T_0 E_m \alpha_m h^2}{100 l^4 q_0}$.

Non-dimensional in-plane stress $\bar{\sigma}_{xx}\left(\frac{L}{2}, +\frac{h}{2}\right) = \frac{L\sigma_{xx}\left(\frac{L}{2}, +\frac{h}{2}\right)}{E_m \alpha_m T_0}$.

Non-dimensional transverse shear stress $\bar{\sigma}_{xy} = \frac{10L\sigma_{xy}}{E_m \alpha_m T_0}$ reported at the upper interface in each case, i.e., at the top surface of the core.

Validation study: For validation study, beam with the following geometric properties are used: L=2 m, b=50 mm, h=200 mm having a thickness scheme of 3-4-3. An udl of the intensity of 5MN/m is applied over the entire length of the beam. The beam is assumed to have S-S ends. For the metal phase, Aluminum (Al) is taken, and for the ceramic phase, Alumina is used $Al: E_m = 70$ GPa, $\nu_m = 0.3$; $Al_2O_3: E_c = 380$ GPa, $\nu_c = 0.3$. Table 1 shows the value of central deflection for the same beam. Present results are compared with those reported by Li *et al.* (2019) using an HSDT-based 2-noded mixed finite element with four d.o.f. per node and Koutoati *et al.* (2021) using CBT and

Table 1 Validation study for displacement (in mm) on 3-4-3 S-S power-law sandwich FGM beams

Beam type	n	Present	Source			
			CBT (Li *et al.* 2019)	CBT (Koutoati *et al.* 2021)	HSDT (Li *et al.* 2019)	HSDT (Koutoati *et al.* 2021)
Type-A	0.5	127.08	124.30	124.31	126.59	126.60
	1	161.35	159.55	159.55	162.00	162.00
	5	279.32	278.29	278.29	281.12	281.12
Type-B	0.5	194.61	189.68	189.68	192.63	192.63
	1	208.42	203.94	203.94	207.31	207.30
	5	231.82	225.80	225.80	230.69	230.68

Table 2 Material properties

Material	Property	P_0	P_{-1}	P_1	P_2	P_3
Metal: Stainless steel ($SUS304$)	$E\ (Pa)$	201.04E9	0	3.079E-4	-6.534E-7	0
	$\alpha\ (K^{-1})$	12.33E-6	0	8.086E-4	0	0
	ν	0.3262	-	-	-	-
Ceramic: Silicon Nitride (Si_3N_4)	$E\ (Pa)$	348.43E9	0	-3.070E-4	2.160E-7	-8.946E-11
	$\alpha\ (K^{-1})$	5.8723E-6	0	9.095E-4	0	0
	ν	0.24	-	-	-	-

HOSDBT with two noded FE having four d.o.f. per node and are found to be in good agreement.

After validating the present model and choosing an appropriate mesh size, sandwich FGM beams' thermal-based bending analysis is carried out. In subsequent studies, the study is carried out on beams made up of different homogenization rules and thickness schemes. For the same, the beam is assumed to be made up of SUS304 (metal) and Si_3N_4 (ceramic). Temperature-dependent material properties are assumed (Table 2).

Type-A sandwich FGM beam: Tables 3, 4, and 5 show the variation of $\bar{w}(l/2,0), \bar{\sigma}_{xx}(l/2,+h/2)$ and $\bar{\sigma}_{xz}$ (at the top interface) respectively, for Type-A S-S sandwich FGM beam subjected to Case A, B, and C thermal loadings for different values of *n*, *a/h* values, and thickness schemes. From tables, the behavior of Type-A sandwich FGM beam under thermal loading depends widely on the temperature at the top and bottom surfaces of the beam, thickness scheme, and geometric property. From Table 3, it is seen that with the increase in temperature at the lower surface from -100 to 200 (Case A to Case C), the value of $\bar{w}$ decreases and the nature of deflection reverses in Case C. For Case B loading, the value of $\bar{w}$ is approximately zero for both H- and S-Type-A beams. For all thickness schemes except 1-8-1, the H-Type-A beam gives a higher value of $\bar{w}$ as compared to S-Type-A beam. Table 4 shows the variation of $\bar{\sigma}_{xx}$ at top of sandwich FGM beam under thermal loadings. In all the cases, the H-Type-A beam gives the negative value of $\bar{\sigma}_{xx}(l/2,+h/2)$ whereas for S-Type-A beam, the same depends on n and thermal loading condition value. For n=0.5 and 1 and Case A loading, the S-Type-A beam gives the positive value of $\bar{\sigma}_{xx}(l/2,+h/2)$ whereas for the remaining cases, a negative value is predicted using the present model. On moving from Case A to C loading, the absolute value of $\bar{\sigma}_{xx}$ increases for both H- and S-Type-A beams. With an increase in value of *n*, the value of $\bar{\sigma}_{xx}$ decreases for Case A and B loadings whereas increases for Case C loading for symmetric thickness scheme for H-Type-A beam. For an unsymmetric H-Type-A beam, the value of $\bar{\sigma}_{xx}$ decreases with an increase in value of n for all types of thermal loading cases. For the S-Type-A beam, with an increase in value of *n*, the value of $\bar{\sigma}_{xx}$ decreases for Case A loading whereas increases for Case B and C loadings. From Table 5, it is observed that the value of $\bar{\sigma}_{xz}$ (at the top interface) decreases with an increase in value of n for Case A loading whereas increases for Case B and C loadings for H-Type-A beam. The same decreases with an increase in value of n for all thermal loading cases for S-Type-A beam. On moving from Case A to Case C loading, the value of $\bar{\sigma}_{xz}$ increases for both H- and S-Type-A beams. Figs. 2 and 3 show the variation of non-dimensional stresses across the thickness of S-S H-Type-A and S-Type-A beams, respectively (1-1-1 thickness scheme, n=2, and L/h=10) for Case A, B, and C loadings using present model. The nature of stress distribution is widely affected by the thermal loading case. The full-beam is divided into 50 layers so that the effective distribution of stresses across the thickness of the beam can be plotted (for all types of beams, i.e., power, exponential, and

Table 3 Non-dimensional central deflection $(\bar{w})$ for S-S Type-A sandwich FGM beam under thermal conditions

L/h	*n*	Loading type	2-1-2	2-1-1	1-1-1	2-2-1	1-2-1	1-8-1
				H-Type-A				
		Case A	0.2599	0.2509	0.2526	0.2439	0.2402	0.1818
	0.5	Case B	-1.4847^{-3}	2.0459^{-2}	1.4197^{-3}	1.7292^{-2}	1.3448^{-3}	-1.1472^{-3}
		Case C	-0.1652	-0.1269	-0.1607	-0.1283	-0.1530	-0.1146
		Case A	0.2849	0.2702	0.2748	0.2613	0.2567	0.1919
50	1	Case B	1.6309^{-3}	2.4441^{-2}	1.5268^{-3}	2.4050^{-2}	1.4119^{-3}	-1.1751^{-3}
		Case C	-0.1809	-0.1327	-0.1746	-0.1283	-0.1638	-0.1212
		Case A	0.3226	0.2984	0.3116	0.2933	0.2878	0.2099
	5	Case B	1.9265^{-3}	2.7148^{-2}	1.7333^{-3}	3.0553^{-2}	-1.5406^{-3}	1.2248^{-3}
		Case C	-0.2055	-0.1467	-0.1987	-0.1385	-0.1829	-0.1339
		Case A	6.5027	6.2762	6.3187	6.1035	6.0092	4.5495
	0.5	Case B	-0.2112	0.5329	-0.2029	0.4546	-0.1923	0.1632
		Case C	-4.1601	-3.1989	-4.0470	-3.2282	-3.8563	-2.8965
		Case A	7.1256	6.7601	6.8725	6.5385	6.4229	4.8026
10	1	Case B	-0.2312	0.6359	-0.2184	0.6264	0.2024	0.1673
		Case C	-4.5500	-3.3387	-4.3929	-3.2232	-4.1234	-3.0623
		Case A	8.0653	7.4624	7.7913	7.3358	7.1968	5.2527
	5	Case B	0.2638	0.7080	0.2468	0.7840	0.2210	0.1747
		Case C	-5.1623	-3.6931	-4.9933	-3.4852	-4.6006	-3.3785
				S-Type-A				
		Case A	0.1930	0.1953	0.1968	0.2006	0.2029	0.2685
	0.5	Case B	1.7378^{-3}	1.7176^{-3}	1.7860^{-3}	-7.6508^{-3}	-0.0114	-2.1524^{-3}
		Case C	-0.1223	-0.1230	-0.1250	-0.1408	-0.1287	-0.1712
		Case A	0.1766	0.1825	0.1821	0.1887	0.1916	0.2540
50	1	Case B	-1.5907^{-3}	-3.7838^{-3}	1.6664^{-3}	-1.4042^{-2}	1.7656^{-3}	-2.1009^{-3}
		Case C	-0.1114	-0.1217	-0.1151	-0.1430	-0.1215	-0.1622
		Case A	0.1494	0.1598	0.1542	0.1630	0.1657	0.2231
	5	Case B	-1.2718^{-3}	-7.9942^{-3}	1.4044^{-3}	-2.1702^{-2}	1.5720^{-3}	-1.9799^{-3}
		Case C	-0.0940	-0.1138	-0.0973	-0.1386	-0.1049	-0.1434
		Case A	4.8213	4.8802	4.9155	5.0111	5.0685	6.7091
	0.5	Case B	-0.2492	0.2463	0.2541	-0.2867	0.3033	-0.3063
		Case C	3.1203	-3.1494	-3.1851	-3.5898	-3.2791	-4.3369
		Case A	4.4134	4.5602	4.5482	4.7132	4.7868	6.3473
10	1	Case B	-0.2298	-0.2450	-0.2376	-0.3974	0.2502	0.2987
		Case C	-2.8494	-3.1158	-2.9399	-3.6487	-3.1000	-4.1119
		Case A	3.7365	3.9973	3.8531	4.0732	4.1400	5.5725
	5	Case B	-0.1875	-0.2376	0.2016	-0.5836	0.2227	-0.2808
		Case C	-2.4165	-2.9101	-2.4967	-3.5337	-2.6858	-3.6440

sigmoidal beams). The present model can predict transverse shear stress-free conditions at the top and bottom surfaces of the beam along with continuity at interfaces. The maximum value of $\bar{\sigma}_{xx}$ and $\bar{\sigma}_{xz}$ is found at interfaces in both cases.

Table 4 Non-dimensional in-plane stress ($\bar{\sigma}_{xx}$) for S-S Type-A sandwich FGM beam under thermal conditions

L/h	*n*	Loading type	2-1-2	2-1-1	1-1-1	2-2-1	1-2-1	1-8-1
					H-Type-A			
		Case A	-21.3401	-22.7239	-23.0591	-24.3483	-25.7817	-39.5553
	0.5	Case B	-63.4547	-58.9548	-64.2776	-60.3246	-65.0526	-67.7050
		Case C	-91.0185	-83.0175	-91.2793	-84.2912	-90.8260	-86.0618
		Case A	-15.5374	-17.9121	-17.9049	-19.9276	-21.9338	-37.1991
50	1	Case B	-61.6106	-56.3271	-62.9319	-57.3514	-64.2109	-67.3534
		Case C	-91.7663	-81.8507	-92.3634	-82.3098	-91.9972	-87.0310
		Case A	-6.7604	-10.9695	-9.3371	-11.9596	-14.7231	-32.9991
	5	Case B	-57.8233	-52.4741	-60.3308	-52.9580	-62.5935	-66.7274
		Case C	-91.4403	-80.2120	-93.7863	-80.4367	-93.8546	-88.9333
		Case A	-4.2454	-4.5094	-4.5882	-4.8335	-5.1315	-7.8934
	0.5	Case B	-12.3527	-11.4497	-12.5197	-11.7322	-12.6907	-13.2809
		Case C	-17.6825	-16.0807	-17.7334	-16.3489	-17.6691	-16.8107
		Case A	-3.0875	-3.5450	-3.5590	-3.9456	-4.3623	-7.4200
10	1	Case B	-11.9615	-10.8950	-12.2232	-11.1137	-12.5024	-13.2016
		Case C	-17.7871	-15.8019	-17.9048	-15.9169	-17.8712	-16.9909
		Case A	-1.3404	-2.1548	-1.8513	-2.3556	-2.9235	-6.5761
	5	Case B	-11.2594	-10.0637	-11.6687	-10.2125	-12.1431	-13.0609
		Case C	-17.7972	-15.3794	-18.1283	-15.5041	-18.1816	-17.3471
					S-Type-A			
		Case A	13.1203	10.0675	14.5209	15.2052	16.7363	40.5790
	0.5	Case B	-23.5677	-30.0925	-22.5953	-25.3846	-66.5789	-15.4172
		Case C	-48.5839	-57.4369	-47.9839	-53.2347	-47.4478	-53.3162
		Case A	7.1155	4.7671	9.1229	10.3869	12.6136	35.3525
50	1	Case B	-26.4652	-34.4138	-24.9421	-29.8570	-23.0142	-16.4247
		Case C	-49.2034	-60.8070	-48.1154	-57.1611	-47.3453	-51.6518
		Case A	-2.8672	-4.1719	-1.0980	0.5890	3.1365	24.4895
	5	Case B	-32.7370	-41.4022	-30.0819	-37.5082	-26.8021	-18.7889
		Case C	-52.6851	-66.1065	-49.6881	-62.9604	-47.2819	-48.5770
		Case A	2.6372	2.0204	2.9156	3.0396	3.3580	8.1331
	0.5	Case B	-4.0688	-5.4088	-3.8969	-4.4604	-12.9709	-2.3306
		Case C	-8.7157	-10.5327	-8.6270	-9.6750	-8.5128	-9.4800
		Case A	1.4374	0.9554	1.8360	2.0683	2.5330	7.0861
10	1	Case B	-4.6690	-6.3126	-4.3974	-5.3804	-4.0071	-2.5563
		Case C	-8.8763	-11.2676	-8.7048	-10.4979	-8.5388	-9.1858
		Case A	-0.5542	-0.8304	-0.2054	0.1060	0.6379	4.8429
	5	Case B	-5.9739	-7.8008	-5.4903	-6.9440	-4.8301	-3.0853
		Case C	-9.6558	-12.4709	-9.1245	-11.7123	-8.6312	-8.6598

Type-B sandwich FGM beam: Table 6 shows the variation of $\bar{w}(l/2,0)$ for S-S Type-B sandwich FGM beam under thermal loadings. The maximum value of $\bar{w}$ for Case A, loading is observed for MT-Type-B beam whereas, for Case B and C loadings, the same is observed for CT-

Table 5 Non-dimensional transverse shear stress $(\bar{\sigma}_{xz})$ for S-S Type-A sandwich FGM beam under thermal conditions

L/h	*n*	Loading type	2-1-2	2-1-1	1-1-1	2-2-1	1-2-1	1-8-1
				H-Type-A				
		Case A	2.0557^{+1}	-0.6984	1.6571^{+1}	4.4005^{+1}	1.1728^{+1}	3.7415
	0.5	Case B	5.2956^{+2}	-1.4933^{+1}	4.0170^{+2}	5.3544^{+2}	2.6335^{+2}	8.5122^{+1}
		Case C	8.2535^{+2}	-2.1356^{+1}	6.2432^{+2}	8.1399^{+2}	4.0839^{+2}	1.2890^{+2}
		Case A	2.0173^{+1}	-2.9074	1.5884^{+1}	5.4967^{+1}	1.1310^{+1}	3.7099
50	1	Case B	5.9090^{+2}	-3.3712^{+1}	4.3093^{+2}	5.7690^{+2}	2.6904^{+2}	8.1310^{+1}
		Case C	9.3063^{+2}	-4.8433^{+1}	6.7826^{+2}	8.7451^{+2}	4.2069^{+2}	1.2345^{+2}
		Case A	2.0552^{+1}	-7.3687	1.4036^{+1}	8.0052	9.4331	3.4886
	5	Case B	6.8538^{+2}	-7.3332^{+1}	4.9169^{+2}	1.4288^{+2}	2.7518^{+2}	7.1384^{+1}
		Case C	1.0789^{+3}	-1.0707^{+2}	7.9315^{+2}	2.5295^{+2}	4.4342^{+2}	1.0913^{+2}
		Case A	6.0049	0.3081	5.2372	1.0878^{+1}	4.0778	1.1772
	0.5	Case B	1.0464^{+2}	-2.8007	7.9434^{+1}	1.0498^{+2}	5.2137^{+1}	1.6695^{+1}
		Case C	1.6207^{+2}	-4.2970	1.2240^{+2}	1.5841^{+2}	7.9880^{+1}	2.5044^{+1}
		Case A	5.3328	-0.2272	4.7188	1.2666^{+1}	3.9234	1.2466
10	1	Case B	1.1673^{+2}	-6.0706	8.5214^{+1}	1.1258^{+2}	5.3321^{+1}	1.5987^{+1}
		Case C	1.8312^{+2}	-8.9368	1.3327^{+2}	1.6966^{+2}	8.2454^{+1}	2.3992^{+1}
		Case A	4.2327	-1.0406	2.9781	2.0271	2.9369	1.2891
	5	Case B	1.3585^{+2}	-1.1410^{+1}	9.7064^{+1}	2.7227^{+1}	5.4607^{+1}	1.4099^{+1}
		Case C	2.1375^{+2}	-1.6771^{+1}	1.5642^{+2}	4.8112^{+1}	8.7353^{+1}	2.1217^{+1}
				S-Type-A				
		Case A	1.1319^{+1}	0.2940	1.0121^{+1}	4.2062	8.5826	4.1593
	0.5	Case B	3.8385^{+2}	2.6394^{+1}	3.4085^{+2}	4.3438^{+2}	2.7918^{+2}	1.4869^{+2}
		Case C	5.9263^{+2}	3.6501^{+1}	5.2374^{+2}	6.6910^{+2}	4.3769^{+2}	2.3136^{+2}
		Case A	1.0237^{+1}	6.3384^{-2}	9.3342	-2.3494	8.3115	4.3977
50	1	Case B	3.5002^{+2}	4.0902^{+1}	3.1695^{+2}	4.3362^{+2}	2.7580^{+2}	1.5349^{+2}
		Case C	5.4062^{+2}	5.9041^{+1}	4.8660^{+2}	6.7605^{+2}	4.2050^{+2}	2.3740^{+2}
		Case A	8.7891	-0.2863	8.1651	-1.1233^{+1}	7.6194	4.8751
	5	Case B	2.7731^{+2}	5.6651^{+1}	2.6499^{+2}	4.6074^{+2}	2.4830^{+2}	1.6060^{+2}
		Case C	4.2927^{+2}	8.3789^{+1}	4.0687^{+2}	7.2711^{+2}	3.7754^{+2}	2.4585^{+2}
		Case A	1.3170	-0.4115	1.0991	-2.3916^{-2}	0.8659	0.4199
	0.5	Case B	7.3022^{+1}	4.3676	6.4990^{+1}	8.2281^{+1}	5.5201^{+1}	2.8491^{+1}
		Case C	1.1339^{+2}	6.3644	1.0048^{+2}	1.2832^{+2}	8.4077^{+1}	4.4615^{+1}
		Case A	1.2872	-0.4062	1.0759	-1.1423	0.8794	0.4132
10	1	Case B	6.6525^{+1}	6.6532	6.0453^{+1}	8.2801^{+1}	5.2647^{+1}	2.9365^{+1}
		Case C	1.0328^{+2}	9.9163	9.3343^{+1}	1.2973^{+2}	8.0790^{+1}	4.5742^{+1}
		Case A	1.5599	-0.2758	1.2457	-2.3695	0.9627	0.4413
	5	Case B	5.2835^{+1}	8.1332	5.0687^{+1}	8.8162^{+1}	4.7490^{+1}	3.0647^{+1}
		Case C	8.1971^{+1}	1.2219^{+1}	7.8109^{+1}	1.3953^{+2}	7.2593^{+1}	4.7295^{+1}

Type-B loading. With an increase in thickness of the core, the value of $\bar{w}$ decreases for n=0.5 and increases for *n*=1 and 5 for CT-Type-B beam for Case A loading. For Case B and C loading, the value of $\bar{w}$ decreases with an increase in thickness of core for CT-Type-B beam. For MT-Type-B

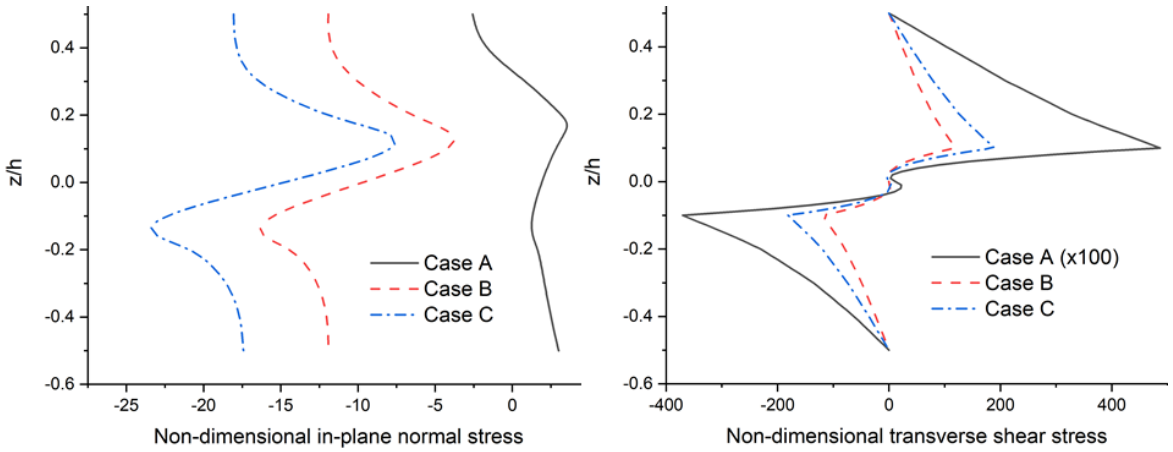

Fig. 2 Variation of non-dimensional stresses across the thickness for 1-1-1 thickness scheme H-Type-A beam having S-S ends (L/h=10, n=2) using present model

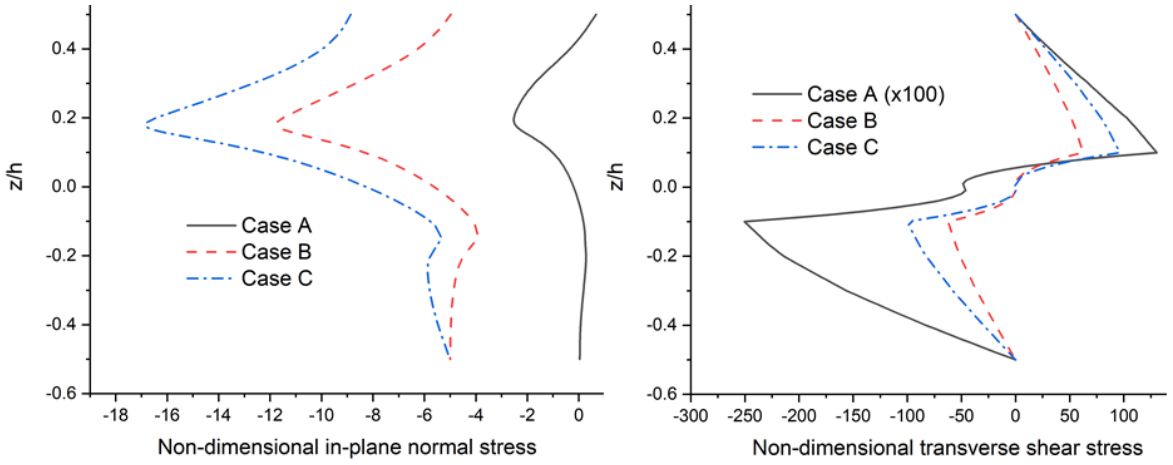

Fig. 3 Variation of non-dimensional stresses across the thickness for 1-1-1 thickness scheme S-Type-A beam having S-S ends (L/h=10, n=2) using present model

beam, the value of $\bar{w}$ increases with an increase in core thickness for n=0.5 and 1 for Case A loading. Thus, it can be stated that the trend of variation of $\bar{w}$ for Type-B beam depends upon the value of temperature at the top and bottom surfaces of the beam and n. Table 7 shows the variation of $\bar{\sigma}_{xx}(l/2, +h/2)$ for Type-B beam. On moving from Case A to C, the value of $\bar{\sigma}_{xx}(l/2, +h/2)$ increases for both CT- and MT-Type-B beam. The nature of $\bar{\sigma}_{xx}$ also depends upon the loading case. Maximum value of $\bar{\sigma}_{xx}(l/2, +h/2)$ is observed for MT-Type-B beam for Case A loading and Case B and C loading for MT-Type-B beam. Table 8 shows the variation of $\bar{\sigma}_{xz}$ (at the top interface) for the same beam. The nature of $\bar{\sigma}_{xz}$ depends upon the loading case and value of n. On moving from Case A to C loading, the value of $\bar{\sigma}_{xz}$ also increases. Generally, it is observed that upon increasing the value of n, the value of $\bar{\sigma}_{xz}$ decreases for CT-Type-B plate and increases for MT-Type-B plate. Figs. 4 and 5 show the variation of non-dimensional stresses across the T-Type-B and MT-Type-B beam's thickness. The nature of the distribution of stresses across the thickness of the

Table 6 Non-dimensional central deflection ($\bar{w}$) for S-S Type-B sandwich FGM beam under thermal conditions

L/h	*n*	Loading type	2-1-2	2-1-1	1-1-1	2-2-1	1-2-1	1-8-1
				CT-Type-B				
		Case A	0.2164	0.2136	0.2159	0.2133	0.2150	0.2106
	0.5	Case B	-7.9562^{-2}	-7.3261^{-2}	-7.7498^{-2}	-7.2955^{-2}	-7.4031^{-2}	-6.3510^{-2}
		Case C	-0.2671	-0.2549	-0.2632	-0.2544	-0.2568	-0.2363
		Case A	0.2165	0.2150	0.2165	0.2148	0.2168	0.2182
50	1	Case B	-7.9887^{-2}	-7.6222^{-2}	-7.8538^{-2}	-7.6200^{-2}	-7.5807^{-2}	-6.7750^{-2}
		Case C	-0.2676	-0.2605	-0.2653	-0.2605	-0.2609	-0.2485
		Case A	0.2166	0.2162	0.2175	0.2162	0.2197	0.2324
	5	Case B	-8.0308^{-2}	-7.8785^{-2}	-7.7706^{-2}	-7.8855^{-2}	-7.3224^{-2}	-5.7776^{-2}
		Case C	-0.2683	-0.2656	-0.2646	-0.2658	-0.2587	-0.2421
		Case A	5.4162	5.3485	5.4047	5.3416	5.3835	5.2733
	0.5	Case B	-2.0355	-1.8996	-1.9912	-1.8957	-1.9108	-1.6610
		Case C	-6.7536	-6.4829	-6.6687	-6.4763	-6.5184	-6.0272
		Case A	5.4203	5.3833	5.4214	5.3794	5.4281	5.4651
10	1	Case B	-2.0576	-1.9752	-2.0246	-1.9805	-1.9598	-1.7799
		Case C	-6.7896	-6.6267	-6.7328	-6.6353	-6.6267	-6.3519
		Case A	5.4266	5.4175	5.4468	5.4169	5.5030	5.8175
	5	Case B	-2.0892	-2.0590	-2.0261	-2.0633	-1.9172	-1.5545
		Case C	-6.8395	-6.7845	-6.7486	-6.7953	-6.6066	-6.2267
				MT-Type-B				
		Case A	0.2207	0.2232	0.2213	0.2232	0.2225	0.2307
	0.5	Case B	8.0083^{-2}	7.3183^{-2}	7.7573^{-2}	7.2739^{-2}	7.3809^{-2}	6.0234^{-2}
		Case C	-1.1661^{-2}	-2.3739^{-2}	-1.5366^{-2}	-2.4653^{-2}	-2.2052^{-2}	-4.8906^{-2}
		Case A	0.2206	0.2219	0.2206	0.2221	0.2208	0.2219
50	1	Case B	7.9887^{-2}	7.5685^{-2}	7.8538^{-2}	7.5172^{-2}	7.5807^{-2}	6.7750^{-2}
		Case C	-1.1813^{-2}	-1.8818^{-2}	-1.3524^{-2}	-1.9817^{-2}	-1.7713^{-2}	-3.1293^{-2}
		Case A	0.2204	0.2205	0.2195	0.2204	0.2173	0.2080
	5	Case B	7.9172^{-2}	7.8746^{-2}	7.6689^{-2}	7.8827^{-2}	7.2232^{-2}	6.0591^{-2}
		Case C	-1.2526^{-2}	-1.3163^{-2}	-1.5544^{-2}	-1.3086^{-2}	-2.1180^{-2}	-3.3987^{-2}
		Case A	5.5311	5.5951	5.5438	5.5986	5.5749	5.7799
	0.5	Case B	2.0727	1.9383	2.0102	1.9268	1.9192	1.6021
		Case C	-0.3630	-0.5466	-0.3851	-0.5676	-0.4942	-1.1793
		Case A	5.5270	5.5638	5.5267	5.5675	5.5310	5.5605
10	1	Case B	2.0576	1.9964	2.0246	1.9826	1.9598	1.7799
		Case C	-0.3544	-0.4244	-0.3638	-0.4471	-0.3925	-0.7418
		Case A	5.5166	5.5292	5.4950	5.5271	5.4428	5.2111
	5	Case B	2.0139	2.0634	1.9583	2.0647	1.8576	1.5765
		Case C	-0.3406	-0.3603	-0.3573	-0.3585	-0.4832	-0.8172

beam widely depends upon the loading Case. However, the nature of stress distribution is similar for Case B and C loadings.

Table 7 Non-dimensional in-plane stress ($\bar{\sigma}_{xx}$) for S-S Type-B sandwich FGM beam under thermal conditions

L/h	*n*	Loading type	2-1-2	2-1-1	1-1-1	2-2-1	1-2-1	1-8-1
					CT-Type-B			
		Case A	16.3219	15.7771	16.3063	15.6888	16.2129	15.2653
	0.5	Case B	-57.8683	-57.7611	-57.4328	-57.5971	-56.3908	-53.4381
		Case C	-105.971	-105.299	-105.202	-105.033	-103.404	-97.8240
		Case A	16.2923	16.0477	16.3919	15.9746	16.6410	17.5756
50	1	Case B	-57.5551	-58.0977	-56.8381	-57.9550	-55.5772	-52.7492
		Case C	-105.462	-106.031	-104.353	-105.801	-102.449	-98.4168
		Case A	16.2295	16.1824	16.6084	16.1582	17.6191	22.9335
	5	Case B	-56.8476	-57.8987	-54.5728	-57.8583	-51.5431	-44.0209
		Case C	-104.315	-105.878	-100.956	-105.851	-96.7736	-88.1918
		Case A	3.2129	3.0996	3.2071	3.0804	3.1856	2.9981
	0.5	Case B	-11.2676	-11.1947	-11.1595	-11.1490	-10.9259	-10.2773
		Case C	-20.6583	-20.4433	-20.4698	-20.3694	-20.0721	-18.8709
		Case A	3.2004	3.1545	3.2199	3.1372	3.2689	3.4544
10	1	Case B	-11.1579	-11.2697	-11.0111	-11.2228	-10.7490	-10.1199
		Case C	-20.4773	-20.6000	-20.2506	-20.5244	-19.8554	-18.9515
		Case A	3.1711	3.1741	3.2493	3.1682	3.4534	4.5196
	5	Case B	-10.9039	-11.1863	-10.4604	-11.1712	-9.8562	-8.2670
		Case C	-20.0619	-20.4962	-19.4112	-20.4790	-18.5803	-16.7337
					MT-Type-B			
		Case A	-25.8467	-25.4265	-25.8369	-25.4197	-25.7523	-24.4927
	0.5	Case B	-39.3187	-39.8004	-39.3333	-39.9090	-39.8430	-43.0433
		Case C	-49.5433	-50.6142	-49.5883	-50.8123	-50.4594	-56.3408
		Case A	-25.9210	-25.6365	-26.0273	-25.6327	-26.1846	-26.3743
50	1	Case B	-39.6939	-39.8482	-39.9385	-40.0196	-40.5790	-43.1436
		Case C	-50.0810	-50.5170	-50.4039	-50.8065	-51.3203	-55.2650
		Case A	-26.0952	-25.9081	-26.5884	-25.9260	-27.4793	-30.4811
	5	Case B	-40.5913	-40.3449	-42.1203	-40.4122	-44.2295	-49.1653
		Case C	-51.3718	-51.1077	-53.4716	-51.1848	-56.2386	-62.1868
		Case A	-5.0465	-4.9571	-5.0527	-4.9574	-5.0393	-4.7925
	0.5	Case B	-7.3821	-7.4043	-7.4053	-7.4343	-7.5079	-8.0933
		Case C	-9.2252	-9.3290	-9.2607	-9.3802	-9.4343	-10.5228
		Case A	-5.0775	-4.9988	-5.1002	-5.0002	-5.1317	-5.1673
10	1	Case B	-7.5246	-7.4304	-7.5720	-7.4753	-7.6933	-8.1568
		Case C	-9.4267	-9.3349	-9.4881	-9.4076	-9.6612	-10.3757
		Case A	-5.1399	-5.0576	-5.2373	-5.0617	-5.4038	-6.0030
	5	Case B	-7.8114	-7.5794	-8.1077	-7.5969	-8.4841	-9.4436
		Case C	-9.8366	-9.5203	-10.2401	-9.5477	-10.7310	-11.8797

Table 8 Non-dimensional transverse shear stress $(\bar{\sigma}_{xz})$ for S-S Type-B sandwich FGM beam under thermal conditions

L/h	*n*	Loading type	2-1-2	2-1-1	1-1-1	2-2-1	1-2-1	1-8-1
				CT-Type-B				
		Case A	-1.2549^{+2}	-5.0720	-6.3665^{+1}	-2.5597^{+1}	-1.4067^{+1}	1.4851
	0.5	Case B	7.9001^{+2}	3.1713^{+1}	4.3596^{+2}	2.3242^{+2}	1.4173^{+2}	6.5880
		Case C	1.2933^{+3}	5.0265^{+1}	7.2102^{+2}	4.0706^{+2}	2.4923^{+2}	1.7298^{+1}
		Case A	-9.5585^{+1}	-9.6903	-6.5821^{+1}	-4.2837^{+1}	-2.8167^{+1}	-0.3549
50	1	Case B	6.1824^{+2}	5.6780^{+1}	4.4728^{+2}	3.2253^{+2}	2.2098^{+2}	2.0613^{+1}
		Case C	1.0195^{+3}	8.9794^{+1}	7.3914^{+2}	5.4861^{+2}	3.7161^{+2}	4.0174^{+1}
		Case A	-7.4106^{+1}	1.0117	-4.0025^{+1}	-4.1029^{+1}	-1.5536^{+1}	-1.5972
	5	Case B	5.0992^{+2}	-5.5231	3.0174^{+2}	2.9747^{+2}	1.3622^{+2}	2.5782^{+1}
		Case C	8.5635^{+2}	-9.5223	5.0797^{+2}	5.0864^{+2}	2.3121^{+2}	4.6239^{+1}
		Case A	-2.5167^{+1}	-1.1686	-1.2923^{+1}	-5.3333	-3.0143	0.3410
	0.5	Case B	1.5523^{+2}	6.3501	8.5819^{+1}	4.6528^{+1}	2.8219^{+1}	1.5163
		Case C	2.5443^{+2}	1.0248^{+1}	1.4218^{+2}	8.1523^{+1}	4.9708^{+1}	3.7052
		Case A	-1.9126^{+1}	-1.9369	-1.3259^{+1}	-8.7269	-5.8040	-0.1475
10	1	Case B	1.2116^{+2}	1.0481^{+1}	8.7706^{+1}	6.4228^{+1}	4.3509^{+1}	4.3099
		Case C	2.0006^{+2}	1.6811^{+1}	1.4517^{+2}	1.0932^{+2}	7.3326^{+1}	8.3325
		Case A	-1.4593^{+1}	0.0192	-8.0692	-8.3427	-3.3524	-0.5374
	5	Case B	9.8728^{+1}	-0.3514	5.8594^{+1}	5.9494^{+1}	2.6532^{+1}	5.0246
		Case C	1.6598^{+2}	-0.3427	9.8860^{+1}	1.0172^{+2}	4.5252^{+1}	9.1450
				MT-Type-B				
		Case A	5.6291^{+1}	0.6026	7.0909^{+1}	1.1755^{+2}	7.1819^{+1}	3.3277^{+1}
	0.5	Case B	2.6539^{+2}	0.9546	3.4266^{+2}	5.8305^{+2}	3.6021^{+2}	1.8952^{+2}
		Case C	3.8728^{+2}	-0.0380	4.9663^{+2}	8.4427^{+2}	5.2043^{+2}	2.7529^{+2}
		Case A	6.0268^{+1}	-0.8344	6.2760^{+1}	1.1528^{+1}	6.9376^{+1}	3.6903^{+1}
50	1	Case B	2.8639^{+2}	-6.4236	3.0010^{+2}	5.4836^{+2}	3.3434^{+2}	1.8640^{+2}
		Case C	4.1972^{+2}	-1.0805^{+1}	4.3677^{+2}	7.9103^{+2}	4.8177^{+2}	2.6773^{+2}
		Case A	-3.5824^{+1}	3.2198	5.4051^{+1}	1.2042^{+2}	1.0410^{+2}	3.8630^{+1}
	5	Case B	-1.0507^{+2}	1.0963^{+1}	2.7316^{+2}	5.3494^{+2}	4.8460^{+2}	1.9449^{+2}
		Case C	-1.1498^{+2}	1.3938^{+1}	4.0701^{+2}	7.6742^{+2}	6.9283^{+2}	2.7847^{+2}
		Case A	1.1163^{+1}	-0.2472	1.3981^{+1}	2.2892^{+1}	1.4142^{+1}	6.5286
	0.5	Case B	5.0160^{+1}	-0.4775	6.5297^{+1}	1.1149^{+2}	6.8901^{+1}	3.6460^{+1}
		Case C	7.2998^{+1}	-0.8039	9.4444^{+1}	1.6133^{+2}	9.9383^{+1}	5.2932^{+1}
		Case A	1.2088^{+1}	-0.4097	1.2517^{+1}	2.2510^{+1}	1.3778^{+1}	7.3093
10	1	Case B	5.4657^{+1}	-1.6048	5.7419^{+1}	1.0495^{+2}	6.4179^{+1}	3.5920^{+1}
		Case C	7.9860^{+1}	-2.5146	8.3341^{+1}	1.5125^{+2}	9.2269^{+1}	5.1515^{+1}
		Case A	-6.7188	0.4554	1.0964^{+1}	2.3662^{+1}	2.0843^{+1}	7.9081
	5	Case B	-2.1244^{+1}	1.5596	5.3067^{+1}	1.0282^{+2}	9.4276^{+1}	3.7901^{+1}
		Case C	-2.3681^{+1}	1.8522	7.8832^{+1}	1.4729^{+2}	1.3446^{+2}	5.4089^{+1}

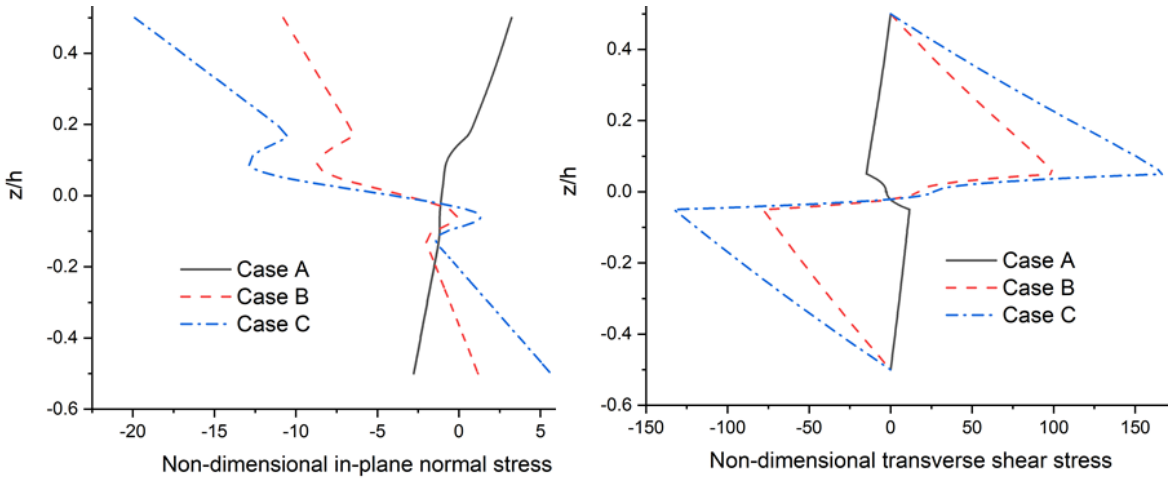

Fig. 4 Variation of non-dimensional stresses across the thickness for 1-1-1 thickness scheme CT-Type-B beam having S-S ends (L/h=10, n=2) using present model

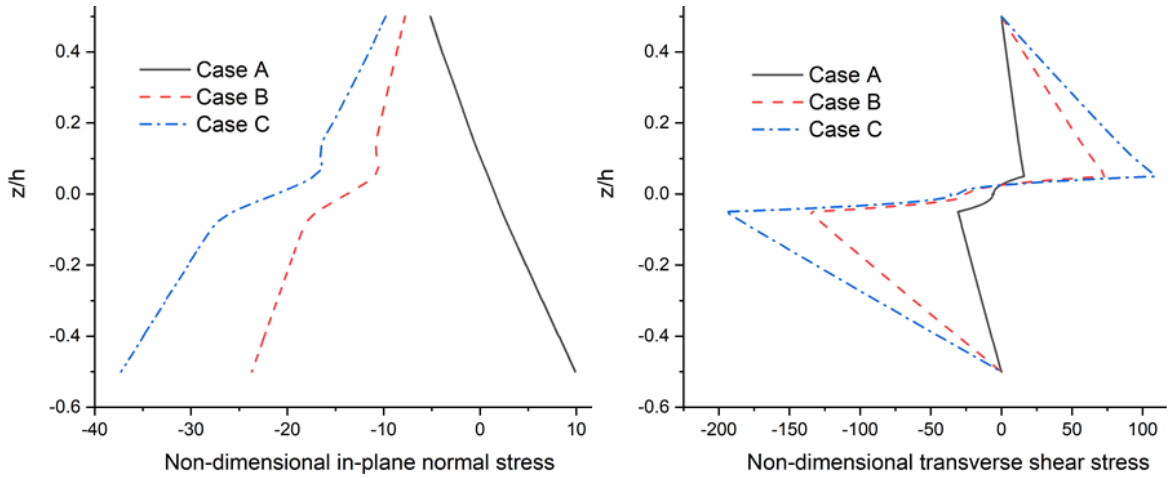

Fig. 5 Variation of non-dimensional stresses across the thickness for 1-1-1 thickness scheme MT-Type-B beam having S-S ends (L/h=10, n=2) using present model

4. Conclusions

In the present study, bending analysis of different kinds of power-law made sandwich FGM beams under bending conditions subjected to thermal loadings. The study has been carried out using analytical solutions based on parabolic shear deformation theory. The present model can predict transverse shear stress-free conditions at the top and bottom surfaces of the beam. Temperature-dependent material properties are taken during the present study. The analysis has been carried out for three different loading conditions: equal rise and fall of temperature at top and bottom surfaces, equal rise or fall of temperature at top and bottom surfaces of the beam, and unequal rise or fall of temperature at the top and bottom surfaces of the beam.

Important points noted during the present study are as follows:

• The maximum stress value is observed at the interface for all types of beams used during the present study.
• The maximum stress value is observed at the interface for all types of beams used during the present study.
• The value of temperature at the top and the bottom surfaces of the beams determines the bending behavior of the beam.
• The value of coefficient 'n' also determines the behavior of the beam.
• Case C loading gives the negative value of displacement for all the thickness schemes and material homogenization rules, and Case A gives the positive value of displacement.
• The highly nonlinear stress distribution is observed across the thickness of the beam, which can be effectively predicted using the present formulation.

Acknowledgments

The research described in this paper received no financial grant in any form.

References

Abualnour, M., Houari, M.S.A., Tounsi, A., Bedia, E.A.A. and Mahmoud, S.R. (2018), "A novel quasi-3D trigonometric plate theory for free vibration analysis of advanced composite plates", *Compos. Struct.*, **184**, 688-697. https://doi.org/10.1016/j.compstruct.2017.10.047.

Akbaş, Ş.D. (2021), "Dynamic analysis of axially functionally graded porous beams under a moving load", *Steel Compos. Struct.*, **39**(6), 811-821. https://doi.org/10.12989/scs.2021.39.6.811.

Almitani, K.H., Eltaher, M.A., Abdelrahman, A.A. and Abd-El-Mottaleb, H.E. (2021), "Finite element based stress and vibration analysis of axially functionally graded rotating beams", *Struct. Eng. Mech.*, **79**(1), 23-33. https://doi.org/10.12989/sem.2021.79.1.023.

Babaei, H., Kiani, Y. and Eslami, M.R. (2018), "Geometrically nonlinear analysis of functionally graded shallow curved tubes in thermal environment", *Thin Wall. Struct.*, **132**, 48-57. https://doi.org/10.1016/j.tws.2018.08.008.

Bekhadda, A., Cheikh, A., Bensaid, I., Hadjoui, A. and Daikh, A.A. (2019), "A novel first order refined shear-deformation beam theory for vibration and buckling analysis of continuously graded beams", *Adv. Aircraft Spacecraft Sci.*, **6**(3), 189-206. https://doi.org/10.12989/aas.2019.6.3.189.

Belarbi, M.O., Tati, A., Ounis, H. and Khechai, A. (2017), "On the free vibration analysis of laminated composite and sandwich plates: a layerwise finite element formulation", *Lat. Am. J. Solid. Struct.*, **14**, 2265-2290. https://doi.org/10.1590/1679-78253222.

Bennai, R., Atmane, H.A. and Tounsi, A. (2015), "A new higher-order shear and normal deformation theory for functionally graded sandwich beams", *Steel Compos. Struct.*, **19**(3), 521-546. https://doi.org/10.12989/scs.2015.19.3.521.

Bouafia, K., Selim, M.M. Bourada, F., Bousahla, A.A. Bourada, M., Tounsi, A., Bedia, E.A.A. and Tounsi A. (2021), "Bending and free vibration characteristics of various compositions of FG plates on elastic foundation via quasi 3D HSDT model", *Steel Compos. Struct.*, **41**(4), 487-503. https://doi.org/10.12989/scs.2021.41.4.487.

Carrera, E. (2003), "Historical review of Zigzag theories for multilayered plates and shells", *Appl. Mech. Rev.*, **56**, 287-308. https://doi.org/10.1115/1.1557614.

Chareonsuk, J. and Vessakosol, P. (2011), "Numerical solutions for functionally graded solids under thermal and mechanical loads using a high-order control volume finite element method", *Appl. Therm. Eng.*, **31**(2-3), 213-227. https://doi.org/10.1016/j.applthermaleng.2010.09.001.

Civalek, Ö. and Demir, Ç. (2011), "Bending analysis of microtubules using nonlocal Euler-Bernoulli beam theory", *Appl. Math. Model.*, **35**(5), 2053-2067. https://doi.org/10.1016/j.apm.2010.11.004.

Di Sciuva, M. and Sorrenti, M. (2021), "Bending and free vibration analysis of functionally graded sandwich plates: An assessment of the Refined Zigzag Theory", *J. Sandw. Struct. Mater.*, **23**(3), 760-802. https://doi.org/10.1177/1099636219843970.

Dorduncu, M. (2020), "Stress analysis of sandwich plates with functionally graded cores using peridynamic differential operator and refined zigzag theory", *Thin Wall. Struct.*, **146**, 106468. https://doi.org/10.1016/j.tws.2019.106468.

Ebrahimi, F., Farazmandnia, N., Kokaba, M.R. and Mahesh, V. (2021), "Vibration analysis of porous magneto-electro-elastically actuated carbon nanotube-reinforced composite sandwich plate based on a refined plate theory", *Eng. Comput.* **37**, 921-936. https://doi.org/10.1007/s00366-019-00864-4.

Esmaeilzadeh, M., Golmakani, M.E., Luo, Y. and Bodaghi, M. (2021), "Transient behavior of imperfect bi-directional functionally graded sandwich plates under moving loads", *Eng. Comput.*, 1-11. https://doi.org/10.1007/s00366-021-01521-5.

Farrokh, M. and Taheripur, M. (2021), "Optimization of porosity distribution of FGP beams considering buckling strength", *Struct. Eng. Mech.*, **79**(6), 711-722. https://doi.org/10.12989/sem.2021.79.6.711.

Filippi, M., Carrera, E. and Zenkour, A.M. (2015), "Static analyses of FGM beams by various theories and finite elements", *Compos. Part B Eng.*, **72**, 1-9. https://doi.org/10.1016/j.compositesb.2014.12.004.

Garg, A. and Chalak, H.D. (2019), "A review on analysis of laminated composite and sandwich structures under hygrothermal conditions", *Thin Wall. Struct.*, **142**, 205-226. https://doi.org/10.1016/j.tws.2019.05.005.

Garg, A. and Chalak, H.D. (2020), "Analysis of non-skew and skew laminated composite and sandwich plates under hygro-thermo-mechanical conditions including transverse stress variations", *J. Sandw. Struct. Mater.*, **23**(8), 3471-3494. https://doi.org/10.1177/1099636220932782.

Garg, A., Belarbi, M.O., Chalak, H.D. and Chakrabarti, A. (2021a), "A review of the analysis of sandwich FGM structures", *Comp. Struct.* **258**, 113427. https://doi.org/10.1016/j.compstruct.2020.113427.

Garg, A., Chalak, H.D. and Chakrabarti, A. (2020a), "Comparative study on the bending of sandwich FGM beams made up of different material variation laws using refined layerwise theory", *Mech. Mater.*, **151**, 103634. https://doi.org/10.1016/j.mechmat.2020.103634.

Garg, A., Chalak, H.D. and Chakrabarti, A. (2020b), "Bending analysis of functionally graded sandwich plates using HOZT including transverse displacement effects", *Mech. Bas. Des. Struct. Mach.*, 1-15. https://doi.org/10.1080/15397734.2020.1814157.

Garg, A., Chalak, H.D., Zenkour, A.M., Belarbi, M.O. and Houari, M.S.A. (2021b), "A review of available theories and methodologies for the analysis of nano isotropic, nano functionally graded, and CNT reinforced nanocomposite structures", *Arch. Comput. Meth. Eng.*, 1-34. https://doi.org/10.1007/s11831-021-09652-0.

Ghannadpour, S.A.M., Mohammadi, B. and Fazilati, J. (2013), "Bending, buckling and vibration problems of nonlocal Euler beams using Ritz method", *Compos. Struct.*, **96**, 584-589. https://doi.org/10.1016/j.compstruct.2012.08.024.

Ghatage, P.S., Kar, V.R. and Sudhagar, P.E. (2020), "On the numerical modelling and analysis of multi-directional functionally graded composite structures: A review", *Compos. Struct.*, **236**, 111837. https://doi.org/10.1016/j.compstruct.2019.111837.

Hadji, L., Amoozgar, M. and Tounsi, A. (2022), "Nonlinear thermal buckling of FG plates with porosity", *Steel Compos. Struct.*, **43**(5), 711-722. https://doi.org/10.12989/scs.2022.42.5.711.

Hosseini, S.A.H., Moghaddam, M.H.N. and Rahmani, O. (2020), "Exact solution for axial vibration of the power, exponential and sigmoid FG nonlocal nanobeam", *Adv. Aircr. Spacecraft Sci.*, **7**(6), 517-536. https://doi.org/10.12989/aas.2020.7.6.517.

Huang, W. and Tahouneh, V. (2021), "Frequency study of porous FGPM beam on two-parameter elastic foundations via Timoshenko theory", *Steel Compos. Struct.*, **40**(1), 139-156. https://doi.org/10.12989/scs.2021.40.1.139.

Kadoli, R., Akhtar, K. and Ganesan, N. (2008), "Static analysis of functionally graded beams using higher order shear deformation theory", *Appl. Math. Model.*, **32**(12), 2509-2525.

https://doi.org/10.1016/j.apm.2007.09.015
Koizumi, M. and Niino, M. (1995), "Overview of FGM Research in Japan", *MRS Bull.*, **20**(1), 19-21. https://doi.org/10.1557/S0883769400048867.
Kouider, D., Kaci, A., Selim, M.M., Bousahla, A.A., Bourada, F., Tounsi, A., Tounsi A. and Hussain M. (2021), "An original four-variable quasi-3D shear deformation theory for the static and free vibration analysis of new type of sandwich plates with both FG face sheets and FGM hard core", *Steel Compos. Struct.*, **41**(2), 167-191. https://doi.org/10.12989/scs.2021.41.2.167.
Koutoati, K., Mohri, F. and Daya, E.M. (2021), "Finite element approach of axial bending coupling on static and vibration behaviors of functionally graded material sandwich beams", *Mech. Adv. Mater. Struct.*, **28**(15), 1537-1553. https://doi.org/10.1080/15376494.2019.1685144.
Li, D. (2020), "Layerwise theories of laminated composite structures and their applications: a review", *Arch. Comput. Meth. Eng.*, **28**, 577-600. https://doi.org/10.1007/s11831-019-09392-2.
Ma, X., Sahmani, S. and Safaei, B. (2021), "Quasi-3D large deflection nonlinear analysis of isogeometric FGM microplates with variable thickness via nonlocal stress-strain gradient elasticity", *Eng. Comput.*, 1-14. https://doi.org/10.1007/s00366-021-01390-y.
Madenci, E. (2021a), "Free vibration and static analyses of metal-ceramic FG beams via high-order variational MFEM", *Steel Compos. Struct.*, **39**(5), 493-509. https://doi.org/10.12989/scs.2021.39.5.493.
Madenci, E. (2021b), "Free vibration analysis of carbon nanotube RC nanobeams with variational approaches", *Adv. Nano Res.*, **11**(2), 157-171. https://doi.org/10.12989/anr.2021.11.2.157.
Madenci, E. and Ozkili, Y.O. (2021), "Free vibration analysis of open-cell FG porous beams: analytical, numerical and ANN approaches", *Steel Compos. Struct.*, **40**(2), 157-173. https://doi.org/10.12989/scs.2021.40.2.157.
Majumdar, A. and Das, D. (2018), "A study on thermal buckling load of clamped functionally graded beams under linear and nonlinear thermal gradient across thickness", *Proc. Inst. Mech. Eng. Part L J. Mater. Des. Appl.*, **232**(9), 769-784. https://doi.org/10.1177/1464420716649213.
Natarajan, S. and Manickam, G. (2012), "Bending and vibration of functionally graded material sandwich plates using an accurate theory", *Finite Elem. Anal. Des.*, **57**, 32-42. https://doi.org/10.1016/j.finel.2012.03.006.
Nejad, M.Z., Hadi, A., Omidvari, A. and Rastgoo, A. (2018), "Bending analysis of bi-directional functionally graded Euler-Bernoulli nano-beams using integral form of Eringen's non-local elasticity theory", *Struct. Eng. Mech.*, **67**(4), 417-425. https://doi.org/10.12989/sem.2018.67.4.417.
Pandey, S. and Pradyumna, S. (2018a), "Transient stress analysis of sandwich plate and shell panels with functionally graded material core under thermal shock", *J. Therm. Stress.*, **41**, 543-567. https://doi.org/10.1080/01495739.2017.1422999.
Pandey, S. and Pradyumna, S. (2018b), "Analysis of functionally graded sandwich plates using a higher-order layerwise theory", *Compos. Part B*, **153**, 325-336. https://doi.org/10.1016/j.compositesb.2018.08.121.
Polat, A. (2021), "Examination of contact problem between functionally graded punch and functionally graded layer resting on elastic plane", *Struct. Eng. Mech.*, **78**(2), 135-143. https://doi.org/10.12989/sem.2021.78.2.135.
Reddy, J.N. (2000), "Analysis of functionally graded plates", *Int. J. Numer. Meth. Eng.*, **47**, 663-684. https://doi.org/10.1002/(SICI)1097-0207(20000110/30)47:1/3<663::AID-NME787>3.0.CO;2-8.
Rezaiee-Pajand, M., Rajabzadeh-Safaei, N. and Masoodi, A.R. (2020), "An efficient curved beam element for thermo-mechanical nonlinear analysis of functionally graded porous beams", *Struct.*, **28**, 1035-1049. https://doi.org/10.1016/j.istruc.2020.08.038.
Sahoo, B., Mehar, K., Sahoo, B., Sharma, N. and Panda, S.K. (2021), "Thermal post‐buckling analysis of graded sandwich curved structures under variable thermal loadings", *Eng. Comput.*, 1-17. https://doi.org/10.1007/s00366-021-01514-4.
Sayyad, A.S. and Ghugal, Y.M. (2019), "Modeling and analysis of functionally graded sandwich beams: a review", *Mech. Adv. Mater. Struct.*, **26**(21), 1776-1795. https://doi.org/10.1080/15376494.2018.1447178.
Shi, G. (2007), "A new simple third-order shear deformation theory of plates", *Int. J. Solid. Struct.*, **44**(13),

4399-4417. https://doi.org/10.1016/j.ijsolstr.2006.11.031.
Singh, P.P. and Azam, M.S. (2021), "Size dependent vibration of embedded functionally graded nanoplate in hygrothermal environment by Rayleigh-Ritz method", *Adv. Nano Res.*, **10**(1), 25-42. https://doi.org/10.12989/ANR.2021.10.1.025.
Tahir, S.I., Tounsi, A., Chikh, A. Al-Osta1, M.A. Al-Dulaijan, S.U. and Al-Zahrani, M.M. (2022), "The effect of three-variable viscoelastic foundation on the wave propagation in functionally graded sandwich plates via a simple quasi-3D HSDT", *Steel Compos. Struct.*, **42**(4), 501-511. https://doi.org/10.12989/scs.2022.42.4.501.
Thai, H.T. and Vo, T.P. (2012), "Bending and free vibration of functionally graded beams using various higher-order shear deformation beam theories", *Int. J. Mech. Sci.*, **62**(1), 57-66. https://doi.org/10.1016/j.ijmecsci.2012.05.014.
Thai, H.T., Nguyen, T.K., Vo, T.P. and Lee, J. (2014), "Analysis of functionally graded sandwich plates using a new first-order shear deformation theory", *Eur. J. Mech.-A/Solid.*, **45**, 211-225. https://doi.org/10.1016/j.euromechsol.2013.12.008.
Tran, T.T., Nguyen, N.H., Do, T.V., Minh, P.V. and Duc, N.D. (2021), "Bending and thermal buckling of unsymmetric functionally graded sandwich beams in high-temperature environment based on a new third-order shear deformation theory" *J. Sandw. Struct. Mater.*, **23**(3), 906-930. https://doi.org/10.1177/1099636219849268.
Wang, H., Zandi, Y., Gholizadeh, M. and Issakhov, A. (2021), "Buckling of porosity-dependent bi-directional FG nanotube using numerical method", *Adv. Nano Res.*, **10**(5), 493-507. https://doi.org/10.12989/anr.2021.10.5.493.
Wattanasakulpong, N., Prusty, G.B. and Kelly, D.W. (2011), "Thermal buckling and elastic vibration of third-order shear deformable functionally graded beams", *Int. J. Mech. Sci.*, **53**(9), 734-743. https://doi.org/10.1016/j.ijmecsci.2011.06.005.
Wattanasakulpong, N., Prusty, G.B. and Kelly, D.W. (2013), "Free and forced vibration analysis using improved third-order shear deformation theory for functionally graded plates under high temperature loading", *J. Sandw. Struct. Mater*., **15**(5), 583-606. https://doi.org/10.1177/1099636213495751.
Wu, C.-P. and Li, E. (2021), "A semi-analytical FE method for the 3D bending analysis of nonhomogeneous orthotropic toroidal shells", *Steel Compos. Struct.*, **39**(3), 291-306. https://doi.org/10.12989/scs.2021.39.3.291.
Yaylaci, M., Yayli, M., Yaylaci, E.U., Olmez H. and Birinci, A. (2021), "Analyzing the contact problem of a functionally graded layer resting on an elastic half plane with theory of elasticity, finite element method and multilayer perceptron", *Struct. Eng. Mech.*, **78**(5), 585-597. https://doi.org/10.12989/sem.2021.78.5.585.
Zhao, J. and Yu, Z. (2021), "On the modeling and simulation of the nonlinear dynamic response of NEMS via a couple of nonlocal strain gradient theory and classical beam theory", *Adv. Nano Res.*, **11**(5), 547-563. https://doi.org/10.12989/anr.2021.11.5.547.

AP